check p_.pdf

Delhi Technological University

Document Details

Submission ID
trn:oid:::27535:101691665

Submission Date
Jun 19, 2025, 8:16 PM GMT+5:30

Download Date
Jun 19, 2025, 8:17 PM GMT+5:30

File Name
check p_.pdf

File Size
2.2 MB

34 Pages

6,228 Words

32,998 Characters

15% Overall Similarity

The combined total of all matches, including overlapping sources, for each database.

Filtered from the Report

- Bibliography
- Quoted Text
- Cited Text

Match Groups

94 Not Cited or Quoted 15%
Matches with neither in-text citation nor quotation marks

0 Missing Quotations 0%
Matches that are still very similar to source material

0 Missing Citation 0%
Matches that have quotation marks, but no in-text citation

0 Cited and Quoted 0%
Matches with in-text citation present, but no quotation marks

Top Sources

10% Internet sources
10% Publications
10% Submitted works (Student Papers)

Integrity Flags

0 Integrity Flags for Review

No suspicious text manipulations found.

Our system's algorithms look deeply at a document for any inconsistencies that would set it apart from a normal submission. If we notice something strange, we flag it for you to review.

A Flag is not necessarily an indicator of a problem. However, we'd recommend you focus your attention there for further review.

Match Groups

- **94** Not Cited or Quoted 15%
  Matches with neither in-text citation nor quotation marks
- **0** Missing Quotations 0%
  Matches that are still very similar to source material
- **0** Missing Citation 0%
  Matches that have quotation marks, but no in-text citation
- **0** Cited and Quoted 0%
  Matches with in-text citation present, but no quotation marks

Top Sources

10% Internet sources
10% Publications
10% Submitted works (Student Papers)

Top Sources

The sources with the highest number of matches within the submission. Overlapping sources will not be displayed.

1	Internet	
espace.curtin.edu.au		<1%
2	Internet	
www.researchgate.net		<1%
3	Submitted works	
Higher Education Commission Pakistan on 2024-08-29		<1%
4	Publication	
Jayaraman Theerthagiri, K. Karuppasamy, C. Justin Raj, Gilberto Maia et al. "Struc...		<1%
5	Internet	
docplayer.net		<1%
6	Internet	
link.springer.com		<1%
7	Internet	
vdoc.pub		<1%
8	Internet	
dr.ntu.edu.sg		<1%
9	Submitted works	
Universiti Putra Malaysia on 2014-10-21		<1%
10	Publication	
Aseel M. Aljeboree, Ayad F. Alkaim, Shaymaa Abed Hussein, Mohammed Abed Ja...		<1%

11 Submitted works
Institute of Graduate Studies, UiTM on 2014-12-24 <1%

12 Publication
Jyotendra Nath, Shashikant Kumar, Vijay Kumar. "Response surface methodology... <1%

13 Publication
Wenli Bai, Hao Yu, Longlong Liu, Esfandiar Pakdel, Bin Tang, Hongli Su, Christoph... <1%

14 Internet
www.jmaterenvironsci.com <1%

15 Submitted works
Indian Institute of Technology, Madras on 2019-01-25 <1%

16 Internet
repositorio.ufsm.br <1%

17 Internet
coek.info <1%

18 Internet
www2.mdpi.com <1%

19 Submitted works
University of Birmingham on 2015-08-25 <1%

20 Internet
mdpi-res.com <1%

21 Publication
Abdul Sameeu Ibupoto, Umair Ahmed Qureshi, Farooq Ahmed, Zeeshan Khatri et ... <1%

22 Publication
Andra-Cristina Enache, Corneliu Cojocaru, Petrisor Samoila, Victor Ciornea et al. "... <1%

23 Submitted works
Sriwijaya University on 2020-04-26 <1%

24 Submitted works
University of Nottingham on 2018-04-17 <1%

25 Internet

www.hindawi.com <1%

26 Publication

"Green Chemistry for Dyes Removal from Wastewater", Wiley, 2015 <1%

27 Publication

Irvan Dahlan, Christopher Chiedozie Obi, Noor Suhaila Razaman, Harahsheh Yaze... <1%

28 Publication

Saptarshi Bose, Binay Kumar Tripathy, Animesh Debnath, Mathava Kumar. "Boos... <1%

29 Internet

www.mdpi.com <1%

30 Internet

www.scielo.br <1%

31 Submitted works

Universiti Sains Malaysia on 2012-06-19 <1%

32 Publication

Yunqing Luo, Shuang Xu, Ao Dou, Zhaolian Han, Tong Zhang, Gaonan Zheng, Lian... <1%

33 Internet

biointerfaceresearch.com <1%

34 Internet

bmccomplementmedtherapies.biomedcentral.com <1%

35 Internet

medwinpublishers.com <1%

36 Internet

pubs.rsc.org <1%

37 Submitted works

BATANGAS STATE UNIVERSITY on 2023-04-06 <1%

38 Submitted works

Higher Education Commission Pakistan on 2013-01-16 <1%

39 Submitted works
Khalifa University of Science Technology and Research on 2025-04-29 <1%

40 Publication
Sarker, Mithun, Biswa Nath Bhadra, Pill Won Seo, and Sung Hwa Jhung. "Adsorpti... <1%

41 Submitted works
Universiti Sains Malaysia on 2013-06-27 <1%

42 Submitted works
University of Sheffield on 2016-09-12 <1%

43 Internet
core.ac.uk <1%

44 Internet
datapdf.com <1%

45 Internet
iwaponline.com <1%

46 Internet
pubs.acs.org <1%

47 Publication
A. Gnanaprakasam, V. M. Sivakumar, M. Thirumarimurugan. "A study on Cu and A... <1%

48 Submitted works
Democritus University on 2025-06-05 <1%

49 Internet
arabjchem.org <1%

50 Internet
escholarship.org <1%

51 Internet
www.ajol.info <1%

52 Internet
www.tandfonline.com <1%

53 Submitted works

7996 on 2015-04-24 <1%

54 Publication

Cui Pang, Yunhai Liu, Xiaohong Cao, Rong Hua, Caixia Wang, Chunqing Li. "Adsor... <1%

55 Submitted works

Institute of Graduate Studies, UiTM on 2014-12-29 <1%

56 Publication

M. Irfan Khan, Teoh. K. Min, Khairun Azizli, Suriati Sufian, Hafeez Ullah, Zakaria M... <1%

57 Internet

hydra.hull.ac.uk <1%

58 Internet

www.nature.com <1%

59 Submitted works

University of Ruhuna Matara on 2025-01-03 <1%

60 Publication

Xin Zhang, Haoyin Zhong, Qi Zhang, Qihan Zhang et al. "High-spin Co3+ in cobalt ... <1%

61 Publication

Ghasem Rezanejade Bardajee, Salameh Azimi, Maryam Bagheri Agha Seyed Shari... <1%

62 Publication

Mohamad Amran Mohd Salleh, Dalia Khalid Mahmoud, Wan Azlina Wan Abdul Ka... <1%

CHAPTER 1

INTRODUCTION AND LITERATURE REVIEW

1.1. Wastewater Treatment

Over the past few decades, environmental issues, particularly those pertaining to the chemical and biological contamination of water, have known to be a significant concern for the ecosystem [1]. Water pollution is increasing day by day because of the discharge of untreated harmful contaminants, like dyes, toxic transition metals, volatile organic compounds, drugs, etc., from paper, printing, textile, and rubber industries, directly into water streams. Among these harmful pollutants, dyes are the one of the most harmful contaminants, which are carcinogenic, mutagenic in nature[2].

Numerous dye-related industries emit effluent that are hazardous to humans and the environment thus deteriorates the quality of life. To reduce its negative impact, dye wastewater requires treatment prior to release into the water stream. To lessen and eliminate the effects, a long-term, effective, and sustainable treatment plan should be developed. Even so, there have been notable developments in the physical, chemical, and biological approaches used to manage and treat this type of wastewater. However, still efforts needs to be done to advance in the area of wastewater treatment technologies[3]. The developed synthesis technique not only helps to the development of sustainable water treatment technologies, but it also offers an advanced alternative for environmental remediation.

1.2. Dyes

Dyes have been around for ages and are crucial part of our everyday lives. After initially relying on insect and the plant sources, the dye industry soon switched to manual

production methods. Sadly, several man-made dyes, particularly the azo dyes, have proven to be toxic and can cause genetic. As a result, they're banned worldwide. Yet , azo dyes are still used and manufactured today because they are cheap and have other useful properties [4].

1.2.1. Classification of Dyes:

Dyes consist of 2 major components among them; one is chromophore that is accountable for its colour and auxochrome is such a component that enhances the color by increasing the stability of dye. Textile industry employs a number of dyes such as basic dyes, acid dyes, reactive dyes, direct dyes, azo dyes, mordant dyes, vat dyes, sulphur dyes and disperse dyes[5]. Presently, the most common class of dyes employed in the sector is azo derivatives[5].The name azo dyes is used to refer to those synthetic organic colorants which are distinguished by having the chromophoric azo group (-N=N-)[5]. Dyes can be classified into cationic and anionic dyes[5]. Cationic dyes are basic dyes whereas the anionic dyes include direct, acid, and reactive dyes[5].

1.2.1.1. Cationic Dyes

Cationic dyes are widely used in the acrylic, wool, nylon and silk dyeing. These dyes are regarded to be toxic colourants and can result in cancer, mutations, skin irritation, and allergic dermatitis[5]. These dyes have varying chemical structures with substituted aromatic groups[6]. In addition to being water soluble and producing coloured cations in solution, cationic dyes have a positive charge within their molecules. Crystal violet, Methylene blue, Brilliant Green, Basic blue, and Basic red are among few of toxic cationic dyes that have been extensively employed as models in dye adsorption studies[5].

1.2.1.2. Anionic Dyes

Anionic dyes are those that contain substances that, when present in an aqueous solution, may lead the dye molecule to break apart into negatively charged ions. This type of dyes contains acidic groups, including sulphate groups and carboxylic groups. Anionic dyes comprise a wide range of compounds from the most diverse dye classes, such as azoic, anthraquinone, triphenylmethane, and nitro dyes, that share the property of water-solubilizing ionic substituents despite having distinctive structural differences [5]. Methyl orange, Congo red, Alizarin red S, Eriochrome Black T are a few of anionic dyes that have been mainly used for research studies on dye adsorption.

Table 1: Formula and Structure of azo dyes[7]

Azo dye	Structure	λ_{max} (nm)	Molecular Formula	Ref.
CV	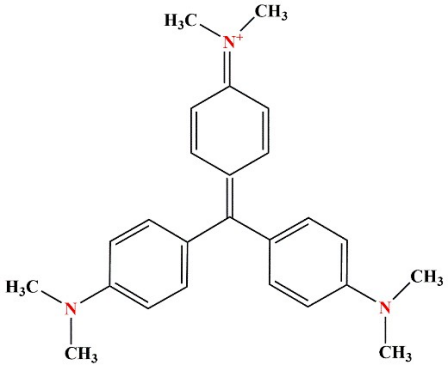	~590 nm	$C_{25}H_{30}N_3Cl$	[8]
BG	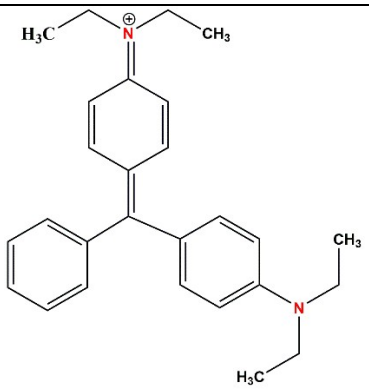	~625 nm	$C_{27}H_{34}N_2O_4S$	[9]

CR	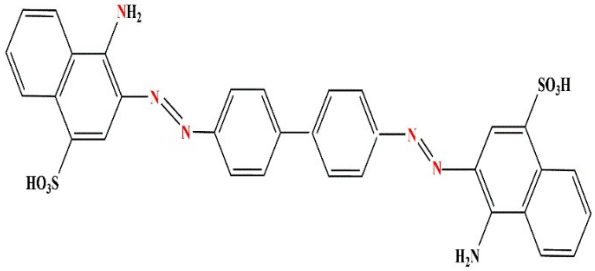	~490 nm	$C_{32}H_{22}N_6Na_2O_6S_2$	[7]
MO	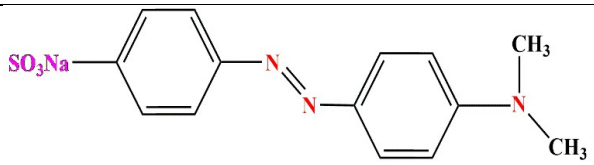	~465 nm	$C_{14}H_{14}N_3NaO_3S$	[10]

1.3. Adsorbents

So far several adsorbents have been reported in the literature for toxic dyes including bio-adsorbents like rice husk[11], charcoal[12], iron oxide[13], zeolite[14], metal oxides[15], alumina[16], alumina with ionic liquid[17], hydroxy apatite[18], chitosan [19], and bone char [20].

1.4. Metal oxyhydroxides

Metal oxyhydroxides (MOOH) comprising p-block or transition(d-block) metals like Al, Ga, Fe, Co, Ni, Zr, and Nb have peculiar electrical characteristics and substantial potential energy storage capacities due to the changing valence states of the Lewis acidic metal [21]. Metal oxyhydroxides are a promising prospect for commercialisation due to their abundance in nature. Among different types of reported adsorbents, MOOH emerges as an excellent adsorbent with characteristics such as area of surface and stability. Area of the surface which is very beneficial for catalytic and adsorption applications because of their special size and composition, having both electric and layered structure numerous applications such as energy storage, lithium-ion batteries, supercapacitors, and biomedical applications and gas sensing.

1.4.1. Synthesis

The fluid-phase techniques, including sol-gel, hydrothermal, solvothermal, electrochemical, precipitation, microwave-assisted, and solution combustion processes, are widely employed [22]. In contrast to fluid-phase methods, a small number of studies focus on solid phase methods (flux-growth, solid-phase combustion, high-temperature pyrolysis, pulsed laser, and MOF(Metal Organic Framework)-derived process) and vapor/gas-phase methods (chemical vapour deposition, atomic layer deposition, spray pyrolysis, plasma process, and magnetron sputtering) [22] for creating MOOHs but create toxic byproducts, require expensive, time-consuming, and energy-intensive procedures, and employ hazardous precursors, which pose serious obstacles to environmental safety and sustainability.

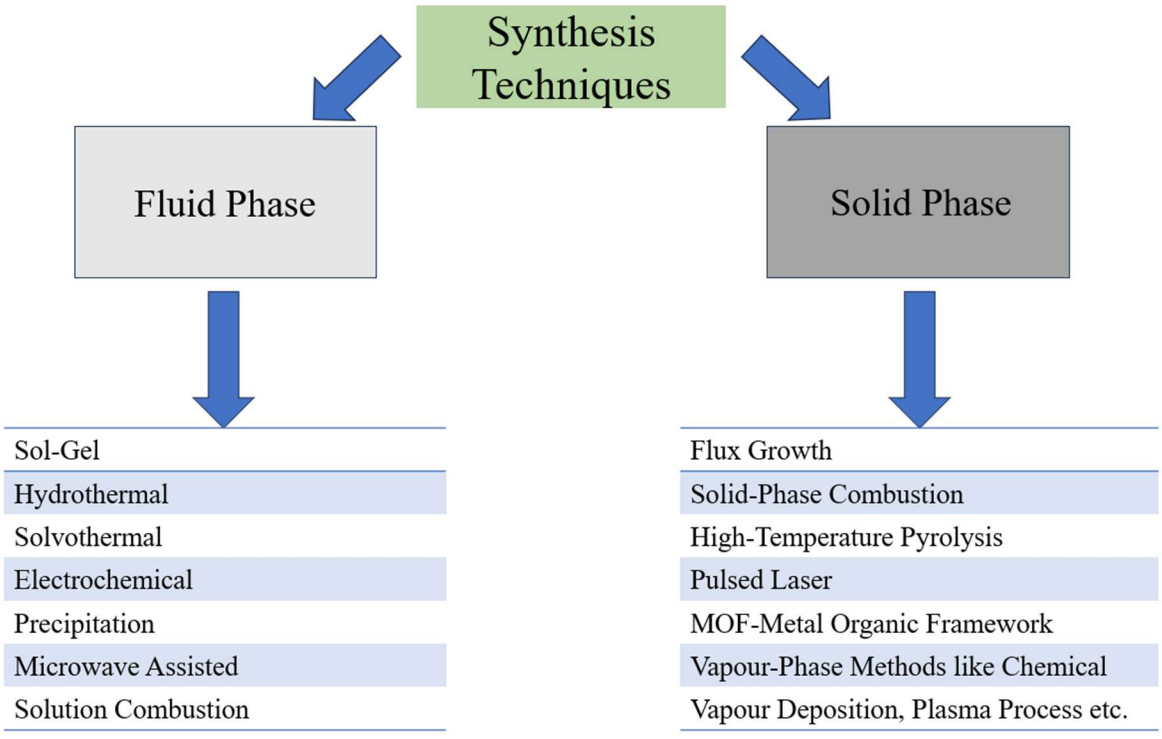

Figure 1. Various Methods of Synthesis of Metal Oxyhydroxides

1.4.2. Applications

Metal oxyhydroxides, a type of transitional metal compound comprises of elements such as cobalt, nickel, manganese, and iron. These nanomaterials work especially well as electrode nanomaterials and electrocatalysts because of their distinct electronic structures and varied valence states.

MOOHs are especially promising in supercapacitor applications. Energy storage devices known as supercapacitors known for having density of high power, a long-life cycle, and the capability to discharge and charge fast enough.

In battery technology, transition metal oxyhydroxides can serve as electrode nanomaterials in alkali metal ion batteries, providing high energy density and cycling stability. They are perfect for next-generation battery applications because of their capacity to go through reversible redox processes, which could lead to performance improvements over conventional materials.

MOOHs are also efficient catalysts for water electrolysis, a method that is essential to the development of clean hydrogen energy that creates hydrogen fuel by separating water into hydrogen and oxygen.

Table 2: Reported literature on synthesis of different metal oxyhydroxides and their applications

MOOH	Synthesis	Application	References
Rice Husk (RH+FeOOH)	Wet chemical method.	Fluoride removal from aqueous media	[23]
CoOOH	Diffusion method	OER electrocatalysts	[24]
VOOH	Hydrothermal method	Water splitting electrocatalysis	[25]
β-Fe/Ni-OOH	Solvothermal method	Electrocatalyst	[26]
SnFe Sulfide/OOH	Solvothermal method	Water splitting electrocatalysis	[27]
Ni/Fe-OOH	one-step wet-chemical synthesis	OER electrocatalysis	[28]
MnCo-OOH	Green synthesis method using alkanna root extract	Electrocatalyst for Enhanced Oxygen Evolution Reaction in Alkaline Medium	[29]
CoOOH	Facile one-pot method	Lithium-ion batteries	[30]
MnOOH	Polyol method	evaluation of their genotoxicity in Vicia faba	[31]
CaOOH	controlled precipitation and polymer complex (Pechini).	to evaluate the capability of degradation of glyphosate-based herbicides (GBH)	[32]

1.5. Cobalt Oxyhydroxide, CoOOH

Cobalt oxyhydroxide (CoOOH), sometimes referred to as cobaltic oxyhydroxide, is a compound with the formula CoOOH and exhibits various forms (α, β and γ) with different crystal structures. Cobalt oxyhydroxide (CoOOH), is defined by the presence of cobalt in its +3-oxidation state. It is a promising catalytic nanomaterial for oxygen evolution reaction (OER) and in the traditional CoOOH structure, Co^{3+} exhibits a low-spin state configuration ($t_{2g}^{6}e_{g}^{0}$), with electron transfer occurring in face-to-face $t_{2g}*$ orbitals [33]. When compared to the low-spin state, high-spin Co^{3+} CoOOH shows better OER activity and faster electron transfer[33].

A naturally occurring mineral, it is a multipurpose substance that can be used as a catalyst, sensor, and energy storage material, among other things. The electrical characteristics and structure of CoOOH have been thoroughly investigated, especially in connection with its function in oxygen evolution reactions and other electrochemical processes.

Chapter 2

EXPERIMENTAL SECTION AND CHARACTERIZATION

2.1 CHEMICALS AND MATERIALS

This research study includes chemicals like Cobalt (II) Acetate Tetrahydrate ($(CH_3COO)_2Co.4H_2O$, Sodium Hydroxide (NaOH), and Hydrogen Peroxide (H_2O_2 30%) of ≥99%. The chemicals used in this study were acquired from MERCK, Germany and employed directly without any other purification. During the whole study, deionised water (DI) water was used. All the solution were freshly prepared for precision and rigorousness just before the experimental procedures.

2.2 METHODOLOGY

2.2.1 Synthesis of Cobalt Hydroxide, $Co(OH)_2$

To synthesise $Co(OH)_2$, an amount of 1.24545g of $(CH_3COO)_2Co.4H_2O$ was dissolved in 100ml of DI water with stirring at 450 rpm until the solution becomes clear. Then, the pH of prepared metal salt solution was adjusted to 10 using 1M NaOH solution (4g NaOH in 100 ml DI water), followed by ultrasonication for 10 minutes. The solution then was filtered and then washed by mixture of DI water and ethyl alcohol to remove impurities. Then, the acquired precipitate was left in oven at 60 ℃ for 24 hours for drying. The dried precipitate then further divided into two parts: the first part was collected as Cobalt Hydroxide ($Co(OH)_2$) product and second part was used for the preparation of Cobalt Oxyhydroxide (CoOOH).

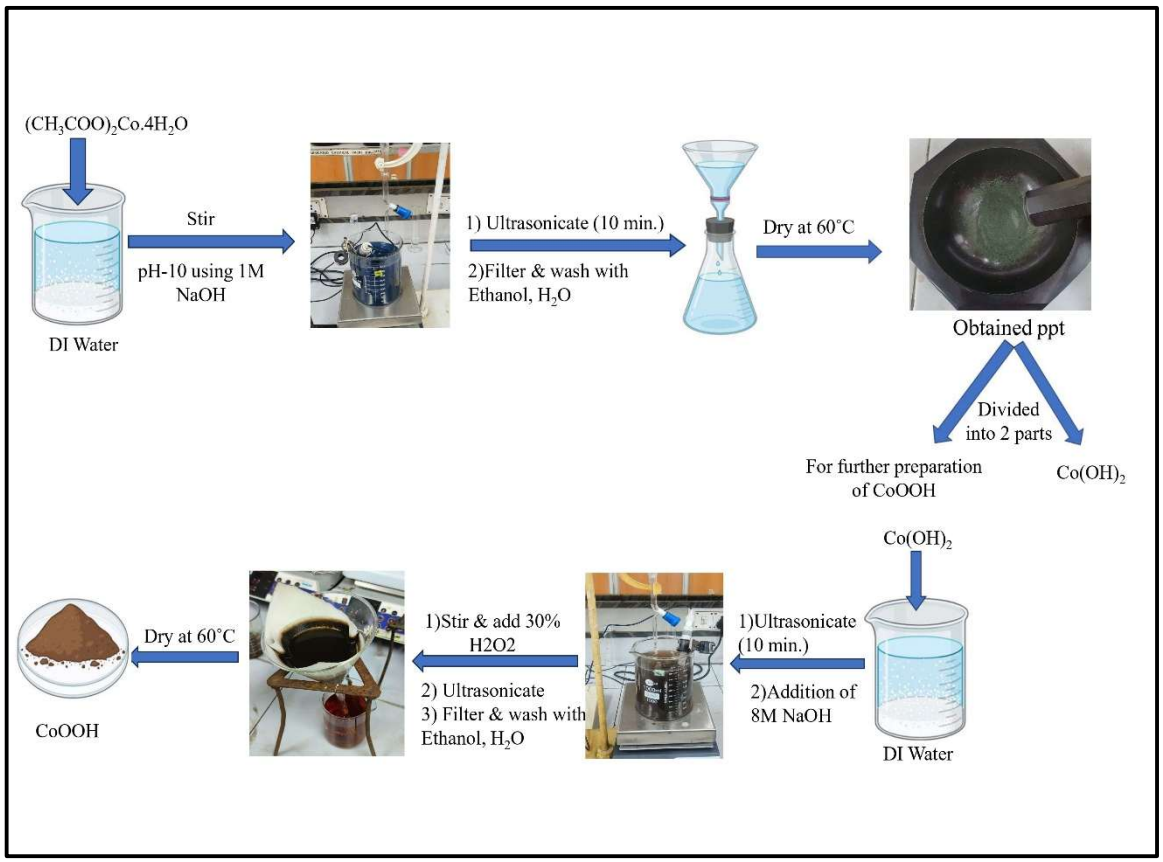

Figure 2. Synthesis of $Co(OH)_2$ and CoOOH

2.2.2 Synthesis of Cobalt Oxyhydroxide, (CoOOH)

The half amount of obtained $Co(OH)_2$ was mixed in 20 ml of deionised water and was further ultrasonicated for 10 minutes, post ultrasonication the dropwise addition of 5 ml of 8M NaOH solution (32g NaOH in 100 ml DI water) was added. Then, the obtained reaction mixture was again stirred for 5 minutes and 2 ml of 30% H_2O_2 solution was added and was then ultrasonicated for 10 minutes. The obtained solution was filtered followed by washing with mixture of DI water with ethanol, and then further dried at 60°C to get CoOOH.

2.3. INSTRUMENTATION

The crystallographic analysis of synthesised CoOOH was culminated through a Powder

X-Ray Diffractometer, namely as Rigaku Minifex-II Model with CuKα radiation. The PXRD patterns were captured within 2θ range of 5° to 90°. Fourier-Transform Infrared Spectroscopy (FTIR), which was recorded using the Perkin-Elmer Spectrum Two Fourier-Transformed Infrared Spectrometer with ranging from 4000-400 cm^{-1} and the KBr disc method, was used for determining the presence of functional groups. With JEOL 7610F Plus, a SEM-EDX examination of the produced nanomaterials was carried out. The Malvern Zeta-Sizer Nano series meter (Version 7.13) was used to measure the synthesized Materials' zeta potential. The nitrogen(N_2) adsorption-desorption technique was used to investigate the average dispersion of pore diameters and specific surface area (S_{BET}) at 77K temperature using the Quanta chromium Nova-1000 equipment.

2.4. ADSORPTION STUDY

Batch-mode studies were conducted to determine the effect of factors like pH, adsorbent dosage, initial dye concentration, contact time, and temperature on the adsorption of Brilliant Green (BG) dye[34]. The influence of such research parameters including the pH (3- 9), adsorbent dosage (50 mg- 200 mg), initial concentration of BG dye (20 mg/L- 50 mg/L), contact time (0-30 minutes), and temperature (303.15 K- 323.15 K) on the efficiency of the adsorption systems was analyzed using the one-factor, one time approach in the dark conditions. For varying the pH of the dye solution, 0.1 M solutions of HCl and NaOH were employed. At every 15-minute intervals, a fixed volume of the solution was collected i.e., 5 ml. Upon completion of the adsorption process, the samples were centrifuged for 5 minutes at 4000 rpm, and the spectra of absorbance was obtained at λ_{max} = 624 nm with the Shimadzu UV-Vis-1900i spectrophotometer.

The removal efficiencyof BG dye and the quantity of dye adsorbed per unit mass of adsorbent (mg/g) at equilibrium and at time t are derived from Equations (2.1), (2.2) and (2.3), respectively.

$$\%\ \boldsymbol{Removal} = \frac{C_i - C_t}{C_i} * \mathbf{100} \qquad \textbf{(2.1)}$$

$$q_e = \frac{C_i - C_e}{W} * V \quad (2.2)$$

$$q_t = \frac{C_i - C_t}{W} * V \quad (2.3)$$

where, C_i, C_t, and C_e correspond to the concentrations of the dye in mg L^{-1} at initial, at time 't', and at equilibrium, respectively. The adsorption capacity is expressed as q_e at equilibrium and q_t at time t both expressed in term mg g^{-1} respectively. The amount of adsorbent and volume of Brilliant Green (BG) dye solution are expressed as W(g) and V(mL).

2.5. Thermodynamic Study

The factors of thermodynamics describe the change in heat, feasibility, and spontaneity of the process for adsorption while selecting a wastewater treatment method. Adsorption experiments were conducted at three temperature values (303.16 K, 313.16 K and 323.16 K) to examine the thermodynamics of the adsorption process. A solution of 20 mg L^{-1} MB dye concentration in 100 mL was agitated with 100 mg adsorbent in the dark at each temperature for 120 minutes to examine the consequence of temperature on the adsorption process. By substituting experimental adsorption data values into standard relationships, Gibbs free energy (ΔG^o, kJ mol^{-1}), enthalpy change (ΔH^o, kJ mol^{-1}), and entropy change (ΔS^o, J mol^{-1} K^{-1}) were determined [7]. The slope and intercept gave the numerical values of ΔH^o and ΔS^o, respectively[35], acquired from a linear plot of $\ln\left(\frac{Q_e}{C_e}\right) vs \left(\frac{1}{T}\right)$ or $lnK_c\ vs \left(\frac{1}{T}\right)$ and the relationship is stated in Eq. (2.4) and (2.5),

$$\ln\left(\frac{Q_e}{C_e}\right) = -\left(\frac{\Delta H^\circ}{RT}\right) + \left(\frac{\Delta S^\circ}{R}\right) \quad (2.4)$$

$$lnK_c = -\left(\frac{\Delta H^\circ}{RT}\right) + \left(\frac{\Delta S^\circ}{R}\right) \quad (2.5)$$

$$K_c = \frac{Q_e}{C_e} \quad (2.6)$$

Here, K_c represents thermodynamic equilibrium constant (L/g) i.e. equal to $\frac{Q_e}{C_e}$, ΔH^o (kJ/mol), ΔS^o (J/(mol K)) states enthalpy and entropy change, respectively, while *R* signifies Gas constant (0.008314 kJ mol^{-1} K^{-1}), and temperature (K) is indicated by T[36]. The change in Gibbs free energy (ΔG^o) predicts if the adsorption process is feasible, as stated by the given equation[37],

$$\Delta G^o = -RT \ln K_c \qquad (2.7)$$

Here, ΔG^o, R, T and ln K_c represent Gibbs free energy change (kJ mol^{-1}), gas constant (kJ mol^{-1} K^{-1}), temperature (K) and thermodynamic equilibrium constant, respectively.

2.6. Reusability

The reusability of CoOOH as an adsorbent is an essential factor confirming the adsorption system's stability. To test its reusability, after the first adsorption cycle, the CoOOH were rinsed with the mixture of water-ethanol and later left in oven to dry at 60°C. The obtained adsorbent was then further reused for subsequent cycles. The process was performed in up to five cycles, and the removal efficacy was estimated after every cycle.

Chapter 3

RESULTS AND DISCUSSION

3.1 Instrumentation:

3.1.1 XRD

The structural identification of Synthesized CoOOH nanomaterials were evaluated through PXRD (Figure 3.1). The CoOOH structure shows characteristic hexagonal PXRD pattern as described in the literature [29]. The strong and intense diffraction peaks appeared at 2θ = 20.484°, 39.18°, 50.60° and 65.79°, corresponding to the *(100)*, *(102)*, *(003)* and *(300)* crystallographic planes, having *d*- spacing values of 4.25 Å, 2.23 Å, 1.80 Å and 1.41 Å.

The average crystalline size (D) of the synthesised nanomaterial was calculated using Debye-Scherrer equation, Equation (3.1),

$$D = \frac{k*\lambda}{\beta*cos\theta} \qquad (3.1)$$

Where, D refers to crystalline diameter, k is the Scherrer constant whose value is 0.94, *l* denotes the incident X-ray wavelength (1.54 Å)[38], β corresponds to the (FWHM) full width at half maximum of peaks and θ indicates diffraction angle. The average crystallite size of synthesised CoOOH nanomaterial was found to be 10.67 nm, thus indicating higher crystallinity and good purity of the synthesised materials.

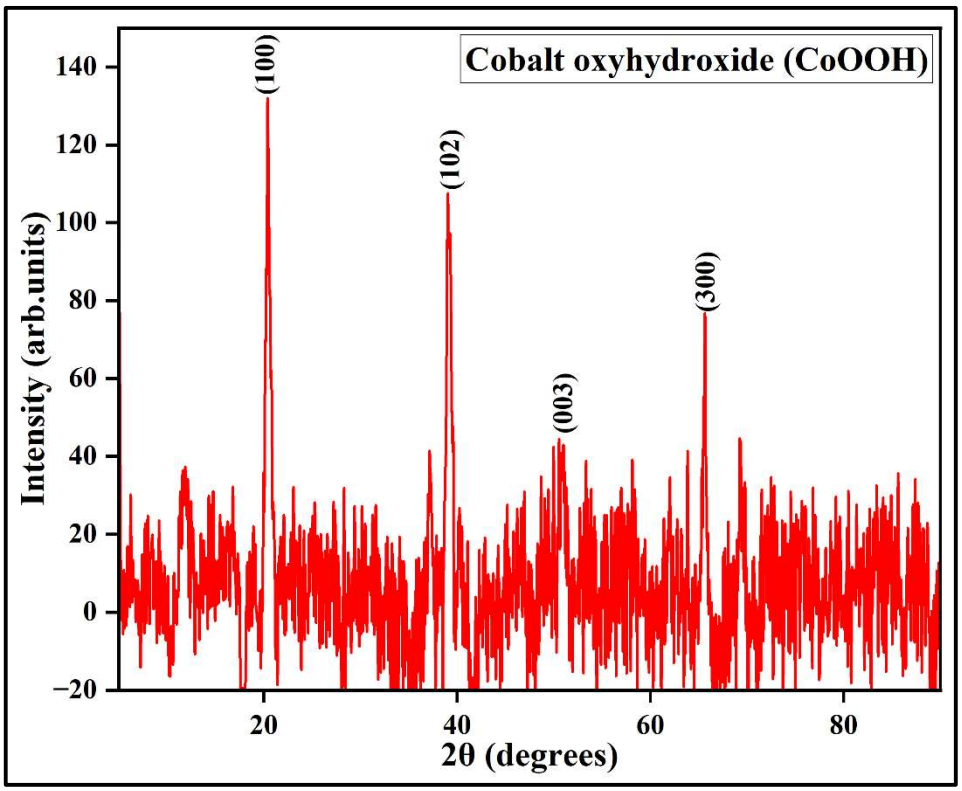

Figure 3. (3.1) PXRD pattern of synthesised CoOOH and (3.2) Comparative PXRD pattern of CoOOH and $Co(OH)_2$

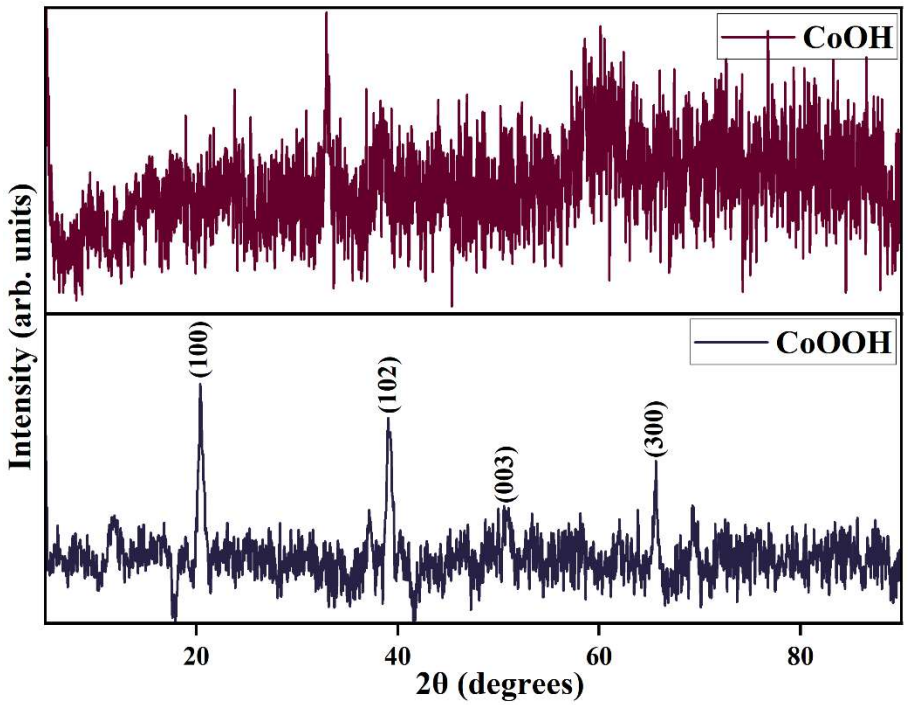

3.1.2. FT-IR

The synthesised nanomaterial was further analysed using FT-IR analysis (400-4000 cm^{-1}), as shown in Figure 4. The broad and intense infrared band at 3454 cm^{-1} correspond to the vibration of stretching of Hydrogen bound O-H. The FTIR peaks at 1632 cm^{-1} and 578 cm^{-1} corresponds to the double and single bonds between Co and O, respectively, thus indicating successful formation of the synthesised CoOOH material[29].

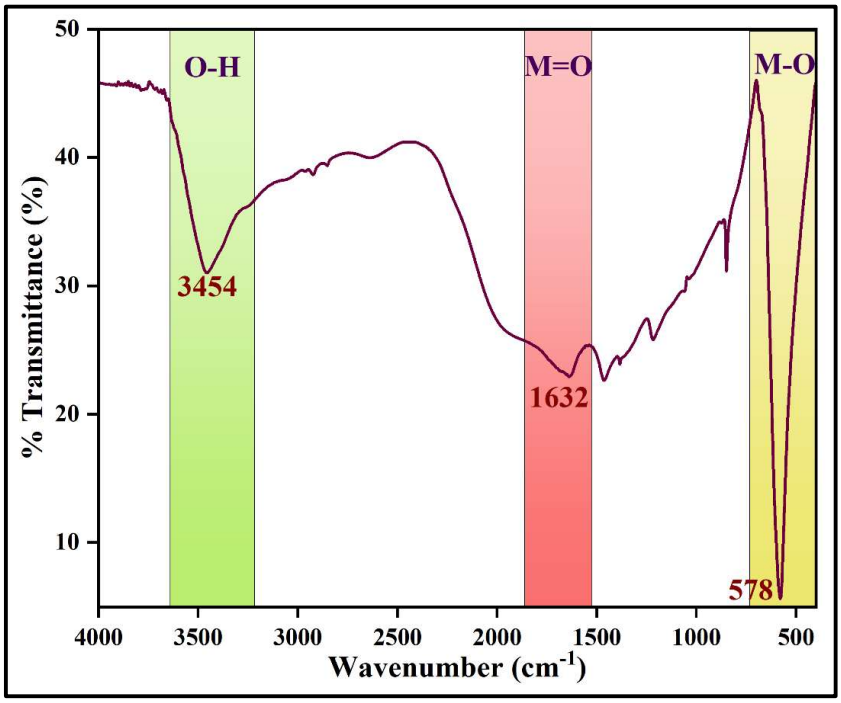

Figure 4. FTIR Spectra of synthesised CoOOH

3.1.3. FE-SEM with EDX

The FE-SEM micrograph of synthesised CoOOH nanomaterial shows flat platelet like structure with uniform distribution of cobalt and oxygen in the synthesised lattice, as shown in figure 5.

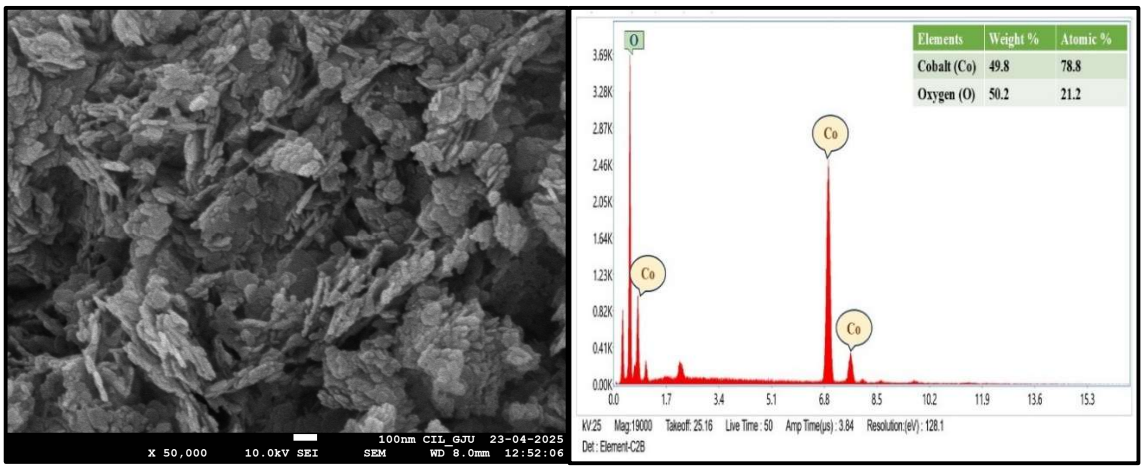

Figure 5. (5.1) FE-SEM micrograph and (5.2) EDX spectra of synthesised CoOOH

3.1.4. BET

Analysis of BET was performed for analysing the specific surface area (S_{BET}), mean pore diameter and pore volume of the synthesised CoOOH nanomaterials. Figure 6 show N_2 desorption-adsorption isotherm of the synthesised CoOOH nanomaterials. The S_{BET} value, mean pore diameter and pore volume for CoOOH nanomaterial was determined to be 36.160 m^2g^{-1}, 0.2928 cc g^{-1}, and 17.2643 nm, respectively. From the results obtained, it was observed that the synthesised nanomaterial possesses increased surface area and pore volume for the adsorption of cationic dye from wastewater. According to the classification of IUPAC, the pattern of the isotherm was similar to be of Type IVa with an H3 hysteresis loop, indicating that the pores have a diameter of more than 2 nm, characteristic of mesoporous nature. As a result, meso-porosity and enhanced surface area of CoOOH contribute to their superior adsorptive properties.

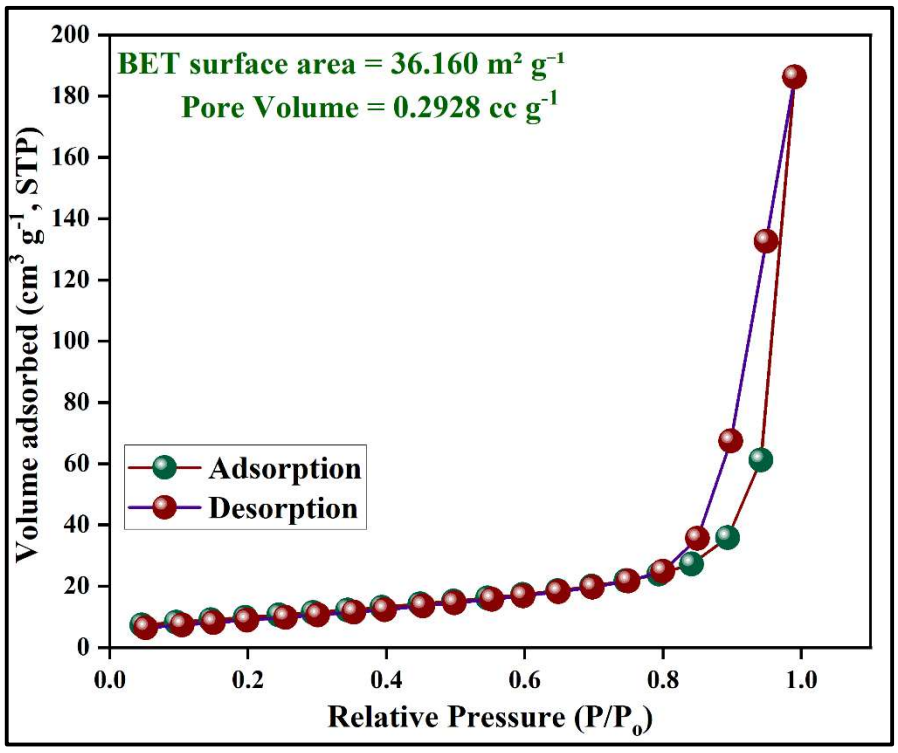

Figure 6. Plot of N_2 Adsorption-desorption isotherm of synthesised CoOOH

3.1.6. Zeta (ζ)-Potential

The dynamic light scattering (DLS) technique was used to produce ζ-potential of the synthesised nanomaterials. The measurement of surface charge of those particle involves ζ-potential, which colloid stability. In this case, CoOOH nanomaterials were found to have ζ-potentials of −34.4 mV in Ethanol solvent, respectively. The obtained values of ζ-potential confirm and justify the hypothesis regarding the possibility of dispersion of the synthesized material. While the CoOOH nanomaterials exhibited negatively charged ζ-potential, indicating strong anionic properties.

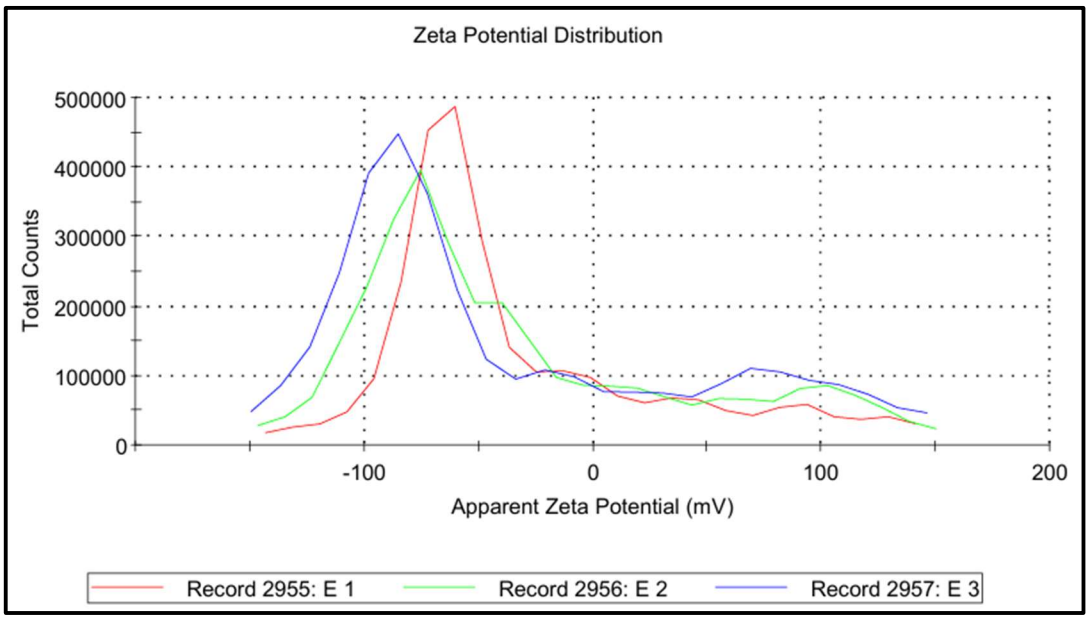

Figure 7. Zeta Potential of CoOOH nanomaterial in Ethanol Solvent

3.2 Batch Adsorption Study

The effectiveness of synthesised Nanomaterials for the adsorption of cationic BG dye from aqueous solution was evaluated using adsorption experiments [39]. The experiments for adsorption were accomplished using aqueous solutions of 100 mL of BG dye (20 mg/L), with 100 mg of CoOOH nanomaterial as adsorbent and were stirred in the dark for 30 minutes. At a regular interval of 2 minutes, a fixed volume of solution was withdrawn, centrifuged for 5 minutes at 4000 rpm, and the concentration of residual solution was estimated using a UV-visible Spectrophotometer at λ_{max}= 624 nm. The findings showed an impressive removal efficiency of 99.45% within 30 minutes, because of good porosity and a larger surface area, surface functionalisation, stabilisation, and efficient dispersibility of the CoOOH materials. Figure 8a shows UV-Visible adsorption spectra for BG dye adsorption using CoOOH nanomaterial as adsorbent at intervals of 2 minutes.

The effectiveness of synthesised Nanomaterials for the adsorption of cationic BG dye from aqueous solution was evaluated using adsorption experiments [39]. The experiments for adsorption were accomplished using aqueous solutions of 100 mL of BG dye (20

mg/L), with 100 mg of CoOOH nanomaterial as adsorbent and were stirred in the dark for 30 minutes. At a regular interval of 2 minutes, a fixed volume of solution was withdrawn, centrifuged for 5 minutes at 4000 rpm, and the concentration of residual solution was estimated using a UV-visible Spectrophotometer at λ_{max}= 624 nm. The findings showed an impressive removal efficiency of 99.45% within 30 minutes, because of good porosity and a larger surface area, surface functionalisation, stabilisation, and efficient dispersibility of the CoOOH materials. Figure 8a shows UV-Visible adsorption spectra for BG dye adsorption using CoOOH nanomaterial as adsorbent at intervals of 2 minutes.

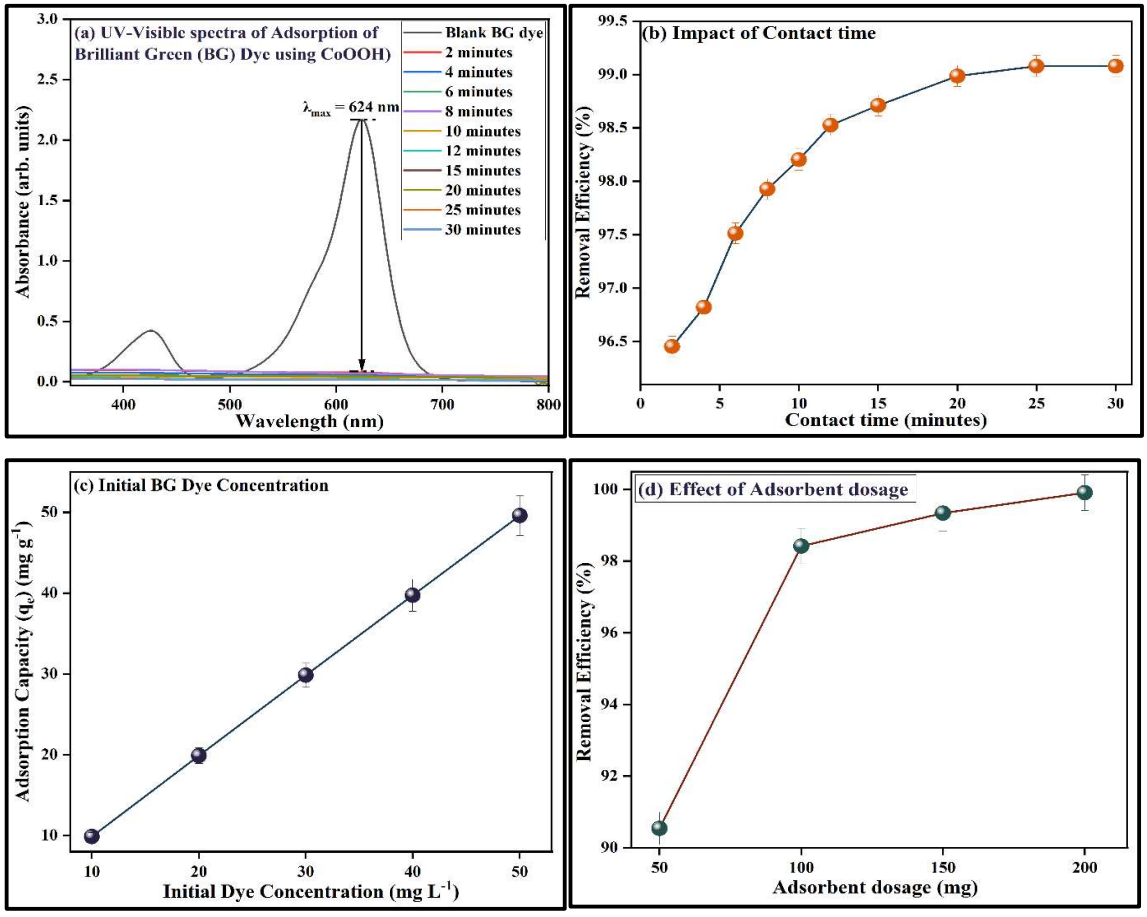

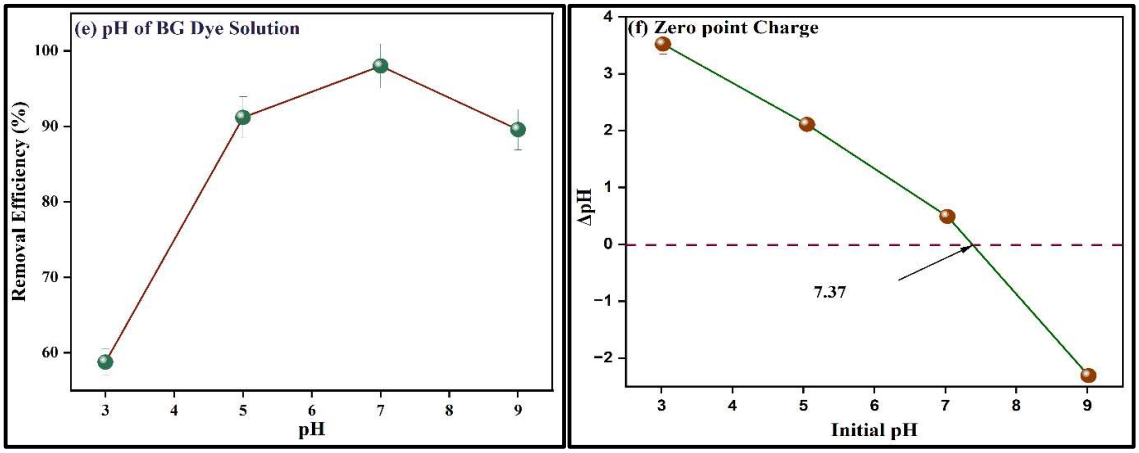

Figure 8. (a) UV-visible adsorption spectra for BG dye adsorption using CoOOH NPs, (b) Influence of contact time on removal efficiency, (c) Influence of dye concentration on adsorption capacity (q_e), (d) Influence of Adsorbent dosage on Removal efficiency of CoOOH NPs, (e) Influence of pH of dye solution on removal efficiency and (f) plot of pH_{zpc} for CoOOH as adsorbent

3.2.1. Effect of Various Influencing Parameters

3.2.1.1. Contact Time

The reaction time between adsorbents and dye pollutants is a crucial factor in adsorption treatment of the wastewater. A 100 mL aqueous solution of BG dye (20 mg L^{-1}) and CoOOH as an adsorbent (100 mg) was employed to examine the impact of reaction time on removal efficiency. Figure 8b shows the removal efficacy (%) plotted against contact time (minutes). The findings indicated that removal efficacy of CoOOH nanomaterial increased rapidly in the first 2 minutes, reaching 96.45 %, and then continued to increase to 98.98 % in the within 20 minutes. However, after 20 minutes, the availability of vacant active adsorption sites decreased, resulting in a minor change in removal efficacy. The equilibrium was observed after 30 minutes, with a maximum removal efficiency of 99.07 %. The rapid initial adsorption is ascribed to electrostatic interactions and intermolecular hydrogen bonding of BG molecules and vacant active adsorption sites on the adsorbent's surface [40].

3.2.1.2. Initial dye concentration

The impact of initial concentration of BG dye on uptake capacity of synthesised CoOOH nanomaterial is shown in Figure 8c. According to the study, when the initial concentration of BG dye raised to 50 mg/L from 20 mg/L, the adsorption capacity of dye raised dramatically to 49.59 mg/g from 19.88 mg/g. This rapid increase in dye uptake capacity is because of improved molecular collisions between the surface of adsorbent and molecules of BG dye, which enhances transfer of mass from solution to solid. Hence, increased molecular collisions lead to enhanced adsorption of molecules from the solution phase.

3.2.1.3. Adsorbent Dose

The influence of adsorbent dosage on removal efficacy of synthesised CoOOH nanomaterial, studied using a 100 ml aqueous solution of BG dye with different doses of CoOOH (50, 100, 150, and 200 mg) while keeping BG concentration (20 mg/L) and contact time (120 mins) constant. The results indicated that when adsorbent dose is increased from 50 mg to 200mg, the removal efficiency of CoOOH increases from 90.54% to 99.91% (Figure 8d). This increase is caused by the CoOOH surface having more active adsorption sites. As a result, 100 mg of adsorbent dosage is optimal for the effective sequestration of BG dye, as increasing the dosage to 150 mg and 200 mg did not yield a significant improvement in removal efficacy, which increased from 98.42% to 99.34% and 99.91%, respectively.

3.2.1.4. Dye Solution pH

The solution’s pH significantly affects the adsorbent's surface charge, which is essential for eliminating dye pollutants from aqueous solutions [37]. The adsorption of BG dye was

examined using a solution with a pH range of 3 to 9. As the pH of solution of dye increases to 5 from 3, removal efficacy of CoOOH nanomaterial also increases from 78.98% to 91.20% (Figure 8e). At lower pH levels, the surface of CoOOH nanomaterial exhibited an increased negative charge, resulting in electrostatic attraction between the negatively charged NPs and the positively charged BG dye molecules (pKa = 4.8)[35]. A correlation exists between dye removal efficiency and pH value, likely attributable to the negative surface charge of the adsorbent under low pH conditions, which interacts with positively charged dye molecules[35]. As the pH increased beyond 7, the removal efficiency declined from 91.20% to 85.59% at pH 9. The observed decrease is due to the deprotonation of surface hydroxyl groups, leading to reduce negative charge on nanomaterial surface, which in turn weakens the electrostatic interaction of surface of adsorption and brilliant green molecules. The efficacy of dye removal diminishes at pH levels exceeding 9, linked to repulsion between the adsorbent surface that is positively charged and methylene blue cations.

Zero-point charge (pH_{zpc}) was studied to estimate the surface charge of the synthesised NPs by employing the salt addition method. In this study, adsorbent (0.02g), added to 20 mL of 0.1 M NaCl solutions with initial pH (pH_i) values modified to 3, 5, 7, 9 and 11, respectively. Afterwards, the solutions were then stirred for 24 hours at ambient temperature. The final pH (pH_f) of the suspension was determined after stirring, and ΔpH was estimated using the formula $\Delta pH = pH_f - pH_i$. The value of pH_{zpc} was estimated from the plot between ΔpH and pH_i at the point where $pH_f = pH_i$ is presented in Figure 8f. The pH_{zpc} value of CoOOH was estimated to be 7.37, indicating that the CoOOHs surface is negatively charged at pH <7.37, promoting electrostatic attraction with the BG molecules and facilitates their adsorption on the surface of the CoOOH. In contrast, at pH > 7.37, the adsorbent's surface acquires a positive charge, repelling BG cations, thereby reducing the removal efficiency at high pH.

3.3. Adsorption Isotherm Study

Isotherm studies provide information about interactions between adsorbent and adsorbate, and determination of maximum dye uptake capacity aids in understanding adsorption mechanisms. Adsorption isotherms were investigated using a 100ml BG dye solution with concentrations ranging between 10 mg L^{-1} and 50 mg L^{-1} and 100 mg adsorbent. Three different models of isotherm were used to analyse the experimental data: Freundlich, Langmuir, and Temkin.

3.3.1. Langmuir:

Langmuir's model states that adsorbed ions bind to the homogeneous surfaces in a monolayer manner. As a result, there are no interactions among the molecules of adsorbent (Figure 9a). The linear regression of Langmuir model is stated in the Eq. (3.2):

$$\frac{C_e}{q_e} = \frac{1}{K_L q_{max}} + \frac{C_e}{q_{max}} \quad \textbf{(3.2)}$$

Where, BG concentration at equilibrium, saturation adsorption capacity, Langmuir constant and maximum BG uptake capacity are represented by C_e (mg/L), q_e (mg/g), k_L (L/mg) and q_{max} (mg/g) respectively.

Another important factor indicating the adsorption process's favourability and irreversibility is separation factor i.e., R_L (constant and dimensionless). The R_L value confirms the validity of the adsorption procedure; R_L= 0 signifies an irreversible reaction, 0< R_L<1 signifies a favourable reaction, R_L >1 signifies an unfavourable reaction, and R_L =1 signifies a linear plot and its relation is given below,

$$R_L = \frac{1}{1+k_L C_0} \quad \textbf{(3.3)}$$

Where, the concentration of BG solution is denoted as by C_o (mg L^{-1}) and the Langmuir constant is represented as k_L (L mg^{-1}).

3.3.2. Freundlich:

This model explains that adsorption takes place on non-uniform adsorptive sites (multilayer adsorption) with non-homogeneous energy distribution.

The linear mathematical equation of the Freundlich model is:

$$\ln q_e = \ln K_f + \frac{1}{n_f} \ln C_e \quad (3.4)$$

Where q_e (mg/g) represents capacity of adsorption at equilibrium, Freundlich coefficients K_f [(mg/g) (L $mg^{-1})^{1/n_f}$] and n_f indicate the adsorbate adsorption capability and heterogenic adsorption intensity and C_e (mg/L) denotes BG concentration at the equilibrium.

The value of the $\frac{1}{n_f}$ factor is a significant parameter for identifying whether the process of adsorption is favorable ($0 < \frac{1}{n_f} < 1$), unfavourable ($\frac{1}{n_f} = 1$), or irreversible ($\frac{1}{n_f} = 0$) and was calculated from the slope of $\ln q_e$ vs $\ln C_e$ plot (Figure 9b).

3.3.3. Temkin:

This model relies on the presumption that solid-solute interactions reduce the amount of heat of adsorption with surface saturation and apply to non-ideal contaminants in the liquid phase and an energetically heterogeneous solid surface. It also demonstrates that the decrease in adsorption heat for the molecules fits the linear pattern, supporting homogeneous binding energy (Figure 9c).

This model can be expressed linearly using Eq. (3.5):

$$q_e = B \ln A_T + B \ln C_e \quad (3.5)$$

$$B = \frac{RT}{b} \quad (3.6)$$

Here q_e (mg/g) represents capacity of adsorption at the equilibrium, B is heat of adsorption constant (J/mol), A_T denotes the Temkin isotherm equilibrium constant, C_e (mg/L)

indicates BG concentration at equilibrium, R i.e., universal gas constant (8.314 J/K/mol), T denotes the absolute temperature (K), and b denotes Temkin isotherm constant (mg L^{-1}).

Figure 9 shows adsorption isotherm models examined for the BG dye's adsorption on CoOOH material, and Table 3 shows calculated values. As a result of the significant correlation between the experimental results and Freundlich isotherm model (R^2 = 0.9565), was assumed that molecules of BG dye were adsorbed uniformly on CoOOH's surface via multilayer adsorption. In addition, the q_{max} i.e., maximum dye capacity was found to be 111.111 mg/g from slope of Langmuir model plot. Furthermore, it was also confirmed that BG dye adsorption onto CoOOH nanomaterialis a favourable method as R_L value falls between 0 and 1, i.e., 0.0243.

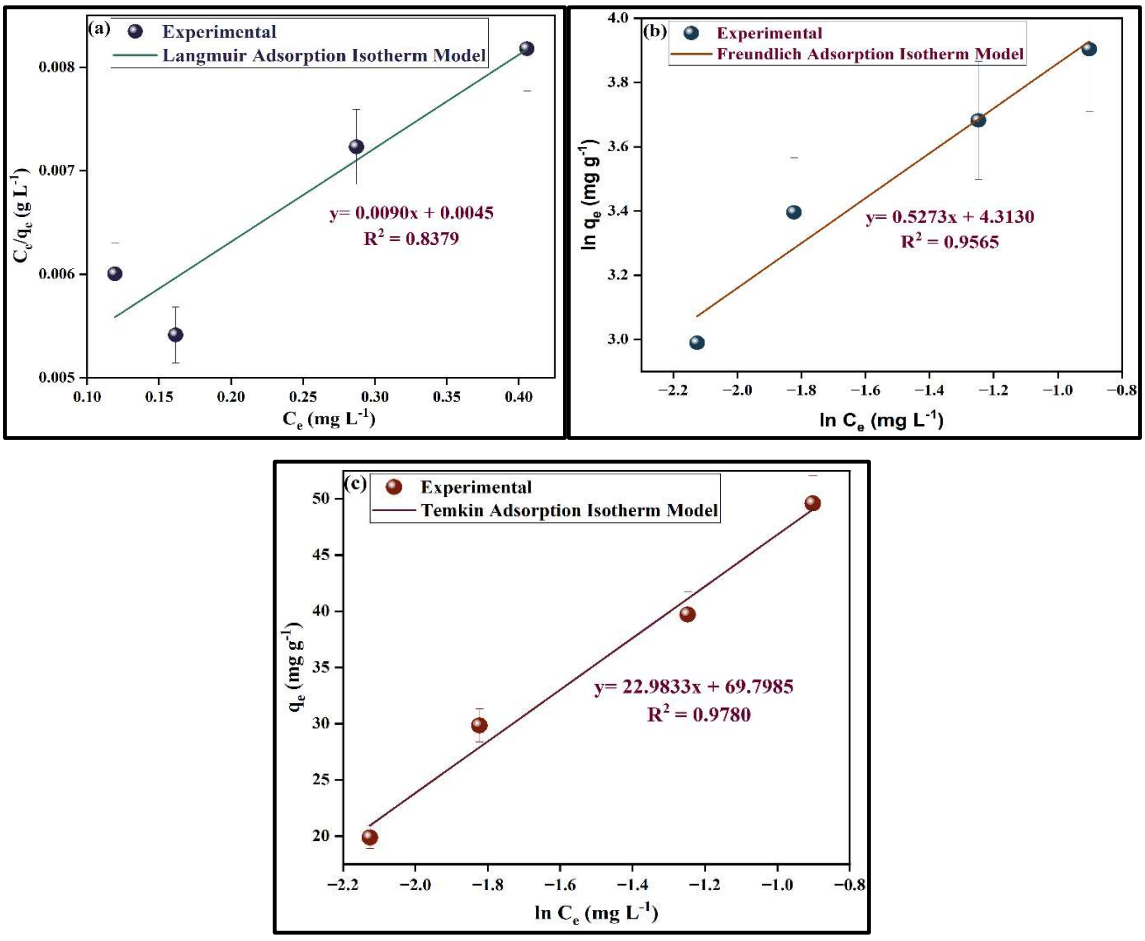

Figure 9. The plots depicting the linear relationships of Langmuir, Freundlich, and Temkin adsorption isotherm mode

Table 3 Compilation of adsorption isotherm parametric values for several mathematical models

Isotherm Models	Linear Plot	Slope and intercept	Parametric Values
Langmuir Model $\frac{C_e}{q_e} = \frac{1}{k_L q_{max}} + \frac{C_e}{q_{max}}$	$\frac{C_e}{q_e}$ vs C_e	Slope = $\frac{1}{q_{max}}$ = 0.0090 Intercept = $(\frac{1}{k_L q_{max}})$ = 0.0045	R^2 = 0.8379 R_L = 0.02439 k_L = 2.00 L mg^{-1} q_{max} = 111.1111 mg g^{-1}
Freundlich Model $\ln q_e = \ln K_f + \frac{1}{n_f} \ln C_e$	$ln\, q_e$ vs $ln\, C_e$	Slope = $\frac{1}{n_f}$ = 0.5273 Intercept = $\ln K_f$ = 4.3130 mg g^{-1}	R^2 = 0.9565 K_f = 74.6641 (mg g^{-1}) (L mg^{-1})$^{1/n}$
Temkin Model $q_e = B \ln A_T + B \ln C_e$	q_e vs ln C_e	Slope = 22.9833 J/mol Intercept = $B \ln A_T$ = 69.7985 mg g^{-1}	R^2 = 0.9780 A_T = 20.7864*10^{-6} L g^{-1}

3.4. Adsorption Kinetic Study

Kinetic studies clarify the mechanisms engaged in the process of adsorption and the adsorption's rate of given system. These studies used CoOOH nanomaterials as an adsorbent (100 mg) in 100 ml of 20 mg/L BG concentration for 30 minutes in the dark. By fitting obtained experimental findings to several kinetic models like pseudo-first-order

(PFO), pseudo-second-order (PSO), and Intraparticle Diffusion (IPD) model, adsorption kinetics for BG dye absorption on CoOOH nanomaterials surface was calculated.

3.4.1. Pseudo-First Order (PFO):

This model signifies a reversible process between BG dye molecules and the adsorbent. The difference in rate of BG dye removal and concentration over time is directly proportional to the change in BG dye uptake at time (t). The linear expression for the PFO model is expressed as:

$$\ln(q_e - q_t) = \ln q_e - k_1 t \quad (3.7)$$

where, adsorbent's dye uptake capacity at the equilibrium and at t time (in minutes) are indicated by q_e, q_t(mg g^{-1}) (Figure 10a). The rate constant of adsorption (min^{-1}) is denoted by k_1.

3.4.2. Pseudo-Second Order (PSO):

Based on this model, rate at which adsorption occurs is influenced by both, concentration of BG dye ions and active adsorption sites present on the CoOOH nanomaterials surface. The linear regression is stated as:

$$\frac{t}{q_t} = \frac{1}{k_2 q_e^2} + \frac{t}{q_e} \quad (3.8)$$

With $$h = k_2 q_e^2 \quad (3.9)$$

Here, adsorption capacity of an adsorbent for dye at time t is expressed by q_t (mg g^{-1}). The rate constant (min^{-1}) is denoted as k_2, q_e (mg/g) denotes the adsorption capacity of dye at the equilibrium and h (mg g/min) denotes the initial adsorption rate (Figure 10b).

3.4.3. Intraparticle Diffusion (IPD):

The PFO and PSO models facilitated the identification of adsorption process; however, due to their inability to elucidate the diffusion mechanism, the IPD model was employed. The linear expression is given by Weber and Morris as follows:

$$q_t = k_{id} t^{1/2} + C \quad (3.10)$$

where q_t (mg/g) represents this uptake capacity of adsorbent for dye at t time, k_{id} is IPD coefficient (g mg^{-1} $min^{-1/2}$), and C indicates the layer thickness of boundary. The values of k_{id} were evaluated using slope of the q_t vs $t^{1/2}$ plot (Figure 10c).

Figure 10 displays the kinetics plots for the models, and Table 4 includes parametric values calculated from linear regressions of above-described models of kinetics. The PSO model has the best correlation with experimental data, $R^2 = 1$, suggesting that the rate of BG adsorption by the synthesised nanomaterials was inferred by chemical adsorption. Eq. (17) was used to derive the parametric value of h, which was assessed as 192.3076 mg g^{-1} min^{-1}.

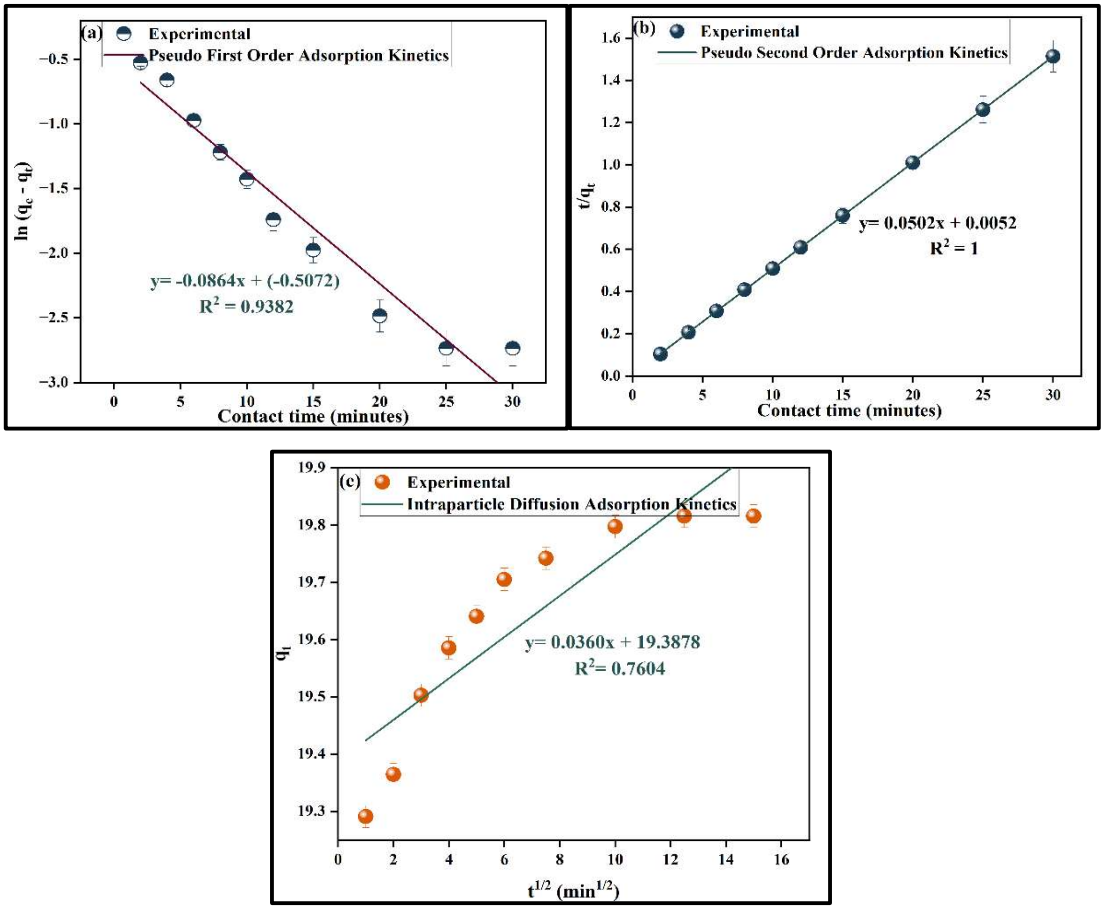

Figure 10. The linear fitted adsorption kinetics curves for BG dye adsorption by CoOOH nanomaterials using PFO, PSO, and IPD model.

Table 4 List of calculated parameters for adsorption kinetics model for BG dye adsorption by CoOOH materials

Kinetic Models	Linear Plot	Slope and Intercept	Parametric Values
Pseudo 1st order $\ln(q_e - q_t) = \ln q_e - k_1 t$	$\ln(q_e - q_t)$ *vs* t	Slope $= -k_1 =$ -0.0864 min^{-1} Intercept = $\ln q_e =$ -0.5072	$R^2 = 0.9382$ $k_1 = 0.0864\ min^{-1}$ $q_e = 0.6021\ mg\ g^{-1}$

Pseudo 2nd order $\frac{t}{q_t} = \frac{1}{k_2 q_e^2} + \frac{t}{q_e}$	$\frac{t}{q_t}$ vs t	Slope $= \frac{1}{q_e} = 0.0502$ Intercept $= \frac{1}{k_2 q_e^2} = 0.0052$	$R^2 = 1$ $k_2 = 0.4846$ min^{-1} h = 192.3076 mg g^{-1} min^{-1} $q_e = 19.9203$ mg g^{-1}
Intraparticle diffusion model $q_t = k_{id}\, t_{1/2} + C$	q_t vs $t_{1/2}$	Slope = k_{id}= 0.0360 Intercept= C = 19.3878	R^2= 0.7604 k_{id} = 0.0360 g mg^{-1}min$^{-1/2}$

3.5. Adsorption Thermodynamics Study

Temperature contributes significantly to the process of adsorption, as removal efficacy of BG dye molecules by the adsorbent varies with temperature. By keeping the adsorbent dose (100 mg), 100 ml aqueous BG dye solution (20 mg/L) and reaction time (120 min.) constant, the consequence of the temperature on the adsorption of BG dye onto the CoOOH surface was examined at 303.15 K, 313.15 K and 323.15 K. The increase in the removal efficacy of CoOOH nanomaterials with increasing temperature is attributed to enhancement in the kinetic energy (K.E) of molecules in solution, leading BG dye molecules to collide with active adsorption sites on the adsorbent surface more frequently at elevated temperatures (Figure 11b).

The adsorption of BG dye on the surface of CoOOH material is an endothermic process, as indicated by the positive ΔH^o value (+ 55.3362 kJ mol^{-1}). Furthermore, this consistent increase in this negative value of ΔG^o with rising temperature (Table 5), indicates that the sequestration rate of BG dye is high at a higher temperature, making the process both thermodynamically feasible and stable. Whereas the increased spontaneity at the BG-nanomaterials interface is evidenced by the positive ΔS^o value (+211.5630 J/mol/K). High activation energy values suggest that adsorption of BG dye molecules onto CoOOH nanomaterials surface occurs via chemical adsorption.

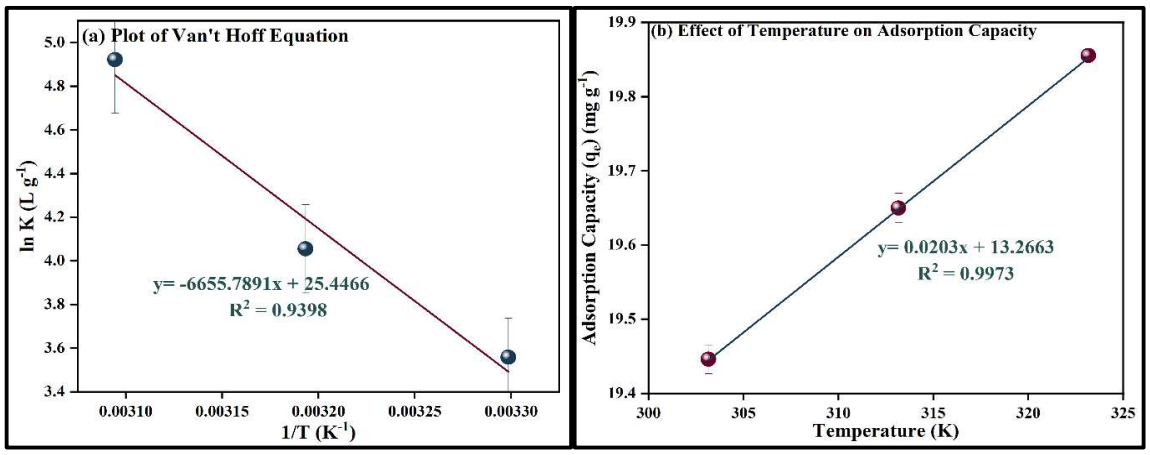

Figure 11. (a) Plot of Van't Hoff equation (ln K vs 1/T), and (b) Impact of temperature on adsorption capacity

Table 5 Thermodynamic parameter value for adsorption of BG dye

Temperature (K)	q_e (mg g^{-1})	ΔH° (kJ/mol)	ΔS° (J/mol/K)	ΔG° (kJ/mol)
303.15	19.247	55.3362	211.5630	-8.166
313.15	19.659			-10.552
323.15	19.791			-12.231

3.3. Recyclability

The adsorption studies were conducted under identical reaction conditions and sustained for a maximum of five cycles to assess regeneration potential of CoOOH when used as adsorbent for the sequestration of BG dye from a dilute solution. CoOOH nanomaterials were centrifuged following the initial adsorption cycle, rinsed with a blend of ethanol and water, then dried at 60°C in oven, and then utilized in the future cycles. The adsorbent was found to be recyclable for up to five adsorption cycles, with adsorption performance assessed for each cycle. The adsorption effectiveness of CoOOH was evaluated at 99.40% in the initial cycle, decreasing to 90.55% after five regeneration cycles, as illustrated in

Figure 11. Consequently, it was determined that the stability and reusability of CoOOH for up to five cycles render it an appropriate option for practical wastewater treatment.

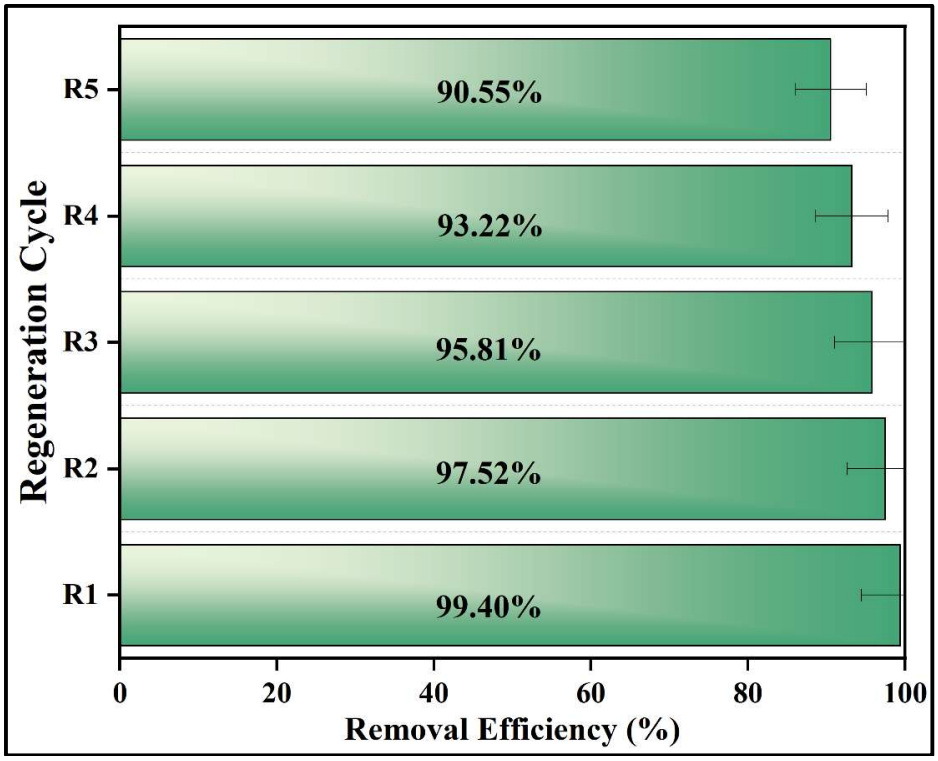

Figure 12. Recyclability of CoOOH for BG dye removal

CHAPTER 4

CONCLUSIONS, FUTURE SCOPE, AND SOCIAL IMPACT

4.1. CONCLUSION

The present work reports the synthesis of cobalt oxyhydroxides (CoOOH) using a ultrasonic assisted synthesis. The synthesized lattice was analysed employing diverse characterisation techniques. Furthermore, the BET analysis was employed to assess the textural characteristics of the synthesized lattice and ascertain its surface area of 36.160 $m^2 g^{-1}$. The produced CoOOH nanomaterial serves as an efficient adsorbent for sequestration of BG dye, with a removal efficiency above 99.40% within 30 minutes [39]. The experimental findings were accurately represented by the Freundlich isotherm and the PSO kinetic model, indicating multilayer adsorption and chemisorption as rate-limiting phase, respectively. Moreover, CoOOH exhibited q_{max} of 111.11 mg g^{-1}. The data indicate that the CoOOH adsorbent may be an efficient option for the BG dye remediation from water solutions. The synthesized adsorbent was effectively utilized for five recycling cycles with good removal efficiency. This study's findings indicate that the CoOOH adsorbent may be an effective alternative for the remediation of BG dye from aqueous media due to its eco-friendliness and affordability. Thus, this study presents novel prospects for the removal of hazardous cationic azo dyes via CoOOH [37].

4.2. FUTURE PROSPECTS

Application research on gas sensors and catalysts

As was previously said, the size effect of the nanomaterial causes it to have a huge surface area and high surface activity. This indicates that the produced nanomaterials have a lot of potential for usage as gas sensors or catalysts. For the nanomaterials to be further modified, the reaction efficiency must be investigated.